Title

Bimodal Mesoporous Titanium Nitride/Carbon Microfibers as Efficient and Stable Electrocatalysts for Li–O2 Batteries

Journal

Chemistry of Materials, 25(19)

ISSN

0897-4756

Authors

Park, Jihee
Jun, Young-Si
Lee, Woo-ram
et al.

Publication Date

2013-10-08

DOI

10.1021/cm401794r

Bimodal Mesoporous Titanium Nitride/Carbon Microfibers as Efficient and Stable Electrocatalysts for Li-O_2 Batteries

Jihee Park,[†] Young-Si Jun,*[† ‡] Woo-ram Lee,[†] Jeffrey A. Gerbec,[‡□] Kimberly A. See, [†§‡] and Galen D. Stucky*[†§‡]

[†]Department of Chemistry and Biochemistry, University of California, Santa Barbara, CA 93106 USA, [§]Materials Department, University of California, Santa Barbara, CA 93106 USA, [‡]Mitsubishi Chemical-Center for Advanced Materials (MC-CAM), University of California, Santa Barbara, CA 93106 USA, [□]Mitsubishi Chemical USA, Chesapeake, VA 23320 USA

KEYWORDS : lithium-air battery, metal nitrides, mesoporous materials, molecular cooperative assembly

The rechargeable Li-O_2 battery has been considered as a sustainable chemical power source for electric vehicles and grid energy storage systems due to the high theoretical specific energy (~3,500 Wh/kg).[1] The practical performance of Li-O_2 batteries is, however, still far below expectations. This is mainly attributed to the 1) intrinsic sluggish reaction kinetics of the oxygen reduction reaction (ORR) and oxygen evolution reaction (OER), 2) passivation of the electrodes by electrical isolation and pore blocking, and 3) chemical instability of the organic cell components, i.e. electrolyte, polymer binder, and carbon electrode, in the presence of $O_2^{\bullet-}$ and Li_2O_2.[2,3] It is crucial to develop highly porous, three-dimensional, conducting cathode catalyst/gas diffusion layer (GDL) architectures possessing superior catalytic activity and stability with respect to the ORR and the OER in order to address these issues.[4] All of these requirements prompted us to examine the catalytic performance of porous framework metal nitride electrodes for Li-O2 batteries.

Non-precious transition metal nitrides have attracted considerable attention as an alternative catalyst to noble metals for electrochemical reactions. Titanium nitride (TiN), in particular, is an interesting material that exhibits excellent thermal, chemical, and mechanical stability, electrical conductivity, and of particular electrocatalytic activity.[5]

TiN is often prepared by the nitridation of titanium oxide using gaseous ammonia or hydrazine as a nitrogen source.[6] This high temperature synthesis, however, gives a material with low surface area, which is unfavorable for its application in heterogeneous electrocatalysis. Recently, mesoporous TiN/carbon composites with high surface areas have been successfully synthesized by using nanostructured graphitic carbon nitride (g-CN) as a reactive template that plays double roles as an exo-template and as a nitrogen (or carbon) source.[7-9] The confined growth enables the formation of small TiN nanoparticles without agglomeration while the decomposition products of g-CN transform the preformed TiO_2 to TiN. One can expect a wide variety of nanostructured TiN/Cs with different structural properties that might be desirable by using other nanostructured g-CNs.[10] The high temperature needed for the synthesis of g-CN, however, limits the possible ways of forming nanostructures mostly because of the templating approach using nanostructured silica. This synthesis procedure is costly and requires multiple steps along with the use of harmful chemicals such as hydrofluoric acid to remove the template. It is, therefore, highly desirable to develop a facile synthesis procedure to shape g-CN or its precursors without using an additional nanocasting template for the large-scale applications of nanostructured TiN.

Recently, we reported the molecular cooperative assembly of g-CN macro-/nanostructures using inexpensive triazines as precursors.[11] The shape and size of the assembly, and thus the resulting g-CN materials, can be tailored simply by using different precipitation temperatures, solvents, and co-monomers. Furthermore, the assembly develops unique nanostructures during the polycondensation without losing the pristine macrostructures. With this in mind we have examined the synthesis of TiN by a molecular cooperative assembly process using the triazines as reactive templates. Amorphous TiO_2 deposited onto the supramolecular networks of melamine and trithiocyanuric acid (MTCA) is converted into a TiN nanocoating after heating at 800°C. This technique yields bimodal mesoporous TiN/C (bmp-TiN/C) microfibers, which provide a catalyst-membrane architecture appropriate for the accommodation of the Li-O_2 discharge product, Li_2O_2, with sizes of a few hundreds of nanometers. The pores allow the efficient mass-transfer of the reactant species, and in addition result in superior catalytic activities for both ORR and OER in Li-O_2 batteries.

A schematic reaction pathway to synthesize bmp-TiN/C using MTCA is described in Figure 1a. MTCA is formed by mixing equimolar solutions of melamine and trithiocyanuric acid in DMSO with water. The spontaneous precipitation yields rectangular microfibers with a length of ~50 μm and a width of ~5 μm. (Figure 1b) The three dimensional structure is constructed *via* hydrogen bonding, electrostatic and π-π interactions between protonated melamine and deprotonated trithiocyanuric acid.

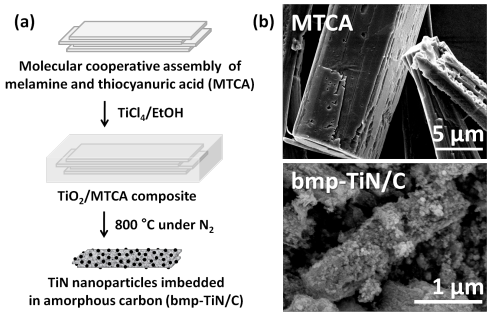

Figure 1 (a) A Schematic reaction pathway to bmp-TiN/C. (b) SEM images of MTCA and bmp-TiN/C.

MTCA is pre-heated to 350°C under air in order to increase the stability of microfibers in the hydrogen bond breaking solvent. It is then mixed with a $TiCl_4$ solution in ethanol and dried at room temperature under air to form amorphous TiO_2 layers on the surface (TiO_2/MTCA composite). The abundant functional groups on the surface of MTCA ensure the stable binding of Ti phases. The TiO_2/MTCA composite is then heated to 800°C under N2. The MTCA within the composite first forms g-CN around 550°C, which is then completely decomposed into NH_3 and CN_x gases above 650°C.[11] These reactive species reduce and convert the TiO_2 to the corresponding nitride. The excess g-CN (or MTCA) is converted into amorphous carbon residues. The onset of two events, i.e. thermal decomposition of g-CN and nitridation of TiO_2, are in the same temperature window, inhibiting the structure collapse that might result from the phase transition of TiO_2 from anatase to rutile. Subsequent heating to 800°C under nitrogen completes the conversion of the surface TiO_2 into the TiN nanoparticles (bmp-TiN/C).

The pristine macrostructure of MTCA is preserved despite structural shrinkage of the overall composite dimensions. (Figure 1b) Residual carbon (29 wt% determined by elemental analysis) likely acts as a binder to preserve the morphology. TEM images and the corresponding electron diffraction pattern of bmp-TiN/C reveal that the resulting material consists of highly crystalline nanoparticles with a size of about 10 nm. (Figure 2a) Indeed, the XRD pattern is in good agreement with that of osbornite, a cubic titanium nitride (JCPDS#01-087-0633). (Figure 2b) The crystal size is estimated to be 9 nm by the Scherrer equation analysis of the (200) diffraction peak profile, coinciding well with the TEM observation. A porous structure is observed in both the TEM and SEM images. (Figure 1b and 2a) N_2 sorption analysis exhibits a surface area of 158 m^2/g and a pore volume of 0.3 cm^3/g. (Figure 2c) The pore size distribution calculated by the BJH method using the desorption branch is bimodal centered at 4 and 50 nm. (Figure 2d) The 4 nm pores are attributed to the interstitial space between the nanoparticles. The 50 nm pores result from the structure contraction of MTCA along with the sheet direction during the polycondensation.

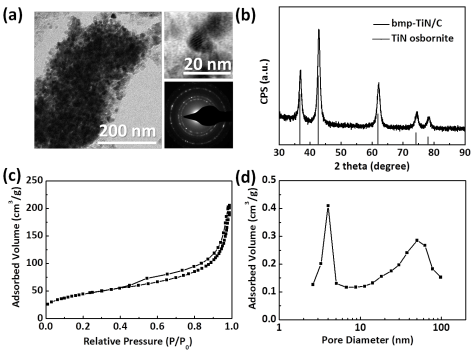

Figure 2 (a) TEM images and the corresponding SAED pattern, (b) XRD pattern, (c) N_2 sorption isotherm, and (d) pore size distribution of bmp-TiN/C.

The electrocatalytic performance of bmp-TiN/C was demonstrated in non-aqueous Li-O_2 batteries using a $LiCF_3SO_3$-tetraethylene glycol dimethyl ether (TEGDME) electrolyte. bmp-TiN/C was first characterized by potentiodynamic cycling with galvanostatic acceleration (PCGA) technique which determines the polarization of the GDL catalyst for oxygen electrochemistry by using a steady-state potential. Figure S1 shows a PCGA profile at a charge capacity of 1,000 mAh/$g_{\text{Super P}}$. Two clear plateaus were observed around 2.6 V and 3.6 V, corresponding to the reversible formation and dissociation of Li_2O_2, respectively. bmp-TiN/C has an ORR potential comparable to those of Super P and Pt/C. The onset potential of OER is at 3.0 V, 100 and 400 mV lower than those of Super P and Pt/C, respectively. The charge profile shows a small step at 3.2 V related to the O_2 release and then slowly increases to 3.76 V. Super P and Pt/C completely recover the charge capacity at 3.84 V and 3.63 V, respectively. The Pt/C cell has an open circuit voltage higher by 400 mV than Super P and bmp-TiN/C cells due to the decomposition of TEGDME by atomic oxygen dissociated by Pt.[12]

In galvanostatic cycling with potential limitation (GCPL) tests of the data shown in Figure 3b, the ORR at a current density of 100 mA/$g_{\text{Super P}}$ occurs at nearly the same potential as that observed in the PCGA analysis. The OER potential is, however, substantially increased mainly due to a large amount of insulating Li_2O_2 being deposited in the pores of the GDL upon discharge. Since the full discharge to 2.0 V deactivates the subsequent charge procedure due to the pore blocking of cathode and thus high polarization resistance (data not shown), the lower cut off potential was set to 2.4 V. The GCPL discharge-charge profile reveals that bmp-TiN/C has a much higher discharge capacity of 19,100±500 mAh/$g_{\text{Super P}}$ compared to

Super P (11,900±600 mAh/$g_{Super\ P}$) and Pt/C (8,100±400 mAh/$g_{Pt/C}$). (Figure 3) It is also notable that bmp-TiN/C alone enables the full discharge-charge cycle with a capacity of 7,100±300 mAh/$g_{bmp\text{-}TiN/C}$ even without including Super P, the ORR catalyst in the final composition. (Figure S2) This strongly suggests that bmp-TiN/C is indeed an efficient catalyst for OER as well as ORR in Li-O_2 battery.

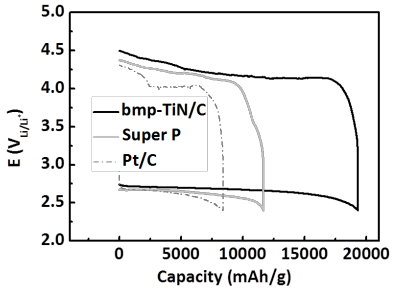

Figure 3 GCPL profiles of bmp-TiN/C, Super P, and Pt/C.

SEM, XRD, and XPS investigations during the discharge-charge cycle confirm the reversible formation of Li_2O_2. (Figure S3) Using bmp-TiN/C without compositing with Super P as a catalyst indicates the target catalyst's ability to achieve the desired electrochemical activity of the ORR and OER. The homogeneous distribution of Li_2O_2 spheres (~700 nm) was observed in the SEM image of GDL after the initial discharge (D1, 25% discharge depth). Furthermore, the peaks in the XRD patterns corresponding to Li_2O_2 systematically increased as the cell was discharged from D1 and D2 (50%) to D3 (80%). Li_2O_2 then mostly disappeared in the SEM image, XRD patterns, and XPS spectra during the subsequent charge procedure. Meanwhile, no oxidation of bmp-TiN/C to TiO_2 was observed in the XRD patterns. These results suggest that the capacity of Li-O_2 cells is mainly through the formation of Li_2O_2.

The cycling stability of bmp-TiN/C was further tested at a lower discharge depth (12%) and higher current density (200 mA/$g_{bmp\text{-}TiN/C}$). Steady cycling is maintained for 35 cycles followed by a rapid fade profile in the bmp-TiN/C cells. (Figure S4) bmp-TiN/C is shown to be chemically and structurally stable after 35 cycles as confirmed by the TEM images, SAED patterns, and XRD peaks. (Figure S5) FT-IR and XPS spectra, however, show that some carbonates are always formed after cycling probably due to the decomposition of amorphous carbon within bmp-TiN/C.[3] (Figure S3c and S6) The increase in the peak intensity at 859 cm^{-1} and 1402 cm^{-1} of FT-IR spectra and 290.4 eV of the XPS spectra implies that the electrode contains carbonates after charging.

In conclusion, bimodal mesoporous TiN/C (bmp-TiN/C) microfibers were successfully synthesized by molecular cooperative assembly using triazines. bmp-TiN/C was characterized by PCGA and GCPL techniques. It was found that bmp-TiN/C forms a catalyst-membrane architecture appropriate for the accommodation of a large amount of Li_2O_2 (19,100±500 mAh/$g_{Super\ P}$) and for the efficient mass-transfer of the electrolyte and oxygen without severe passivation by Li_2O_2. Additionally the catalyst is stable against $O_2^{\bullet-}$ and Li_2O_2 and efficient for both ORR and OER in Li-O_2 cells as compared to the commercial catalysts, Super P and Pt/C. Although residual carbon within bmp-TiN/C is potentially decomposing during cycling, the carbon content can be varied easily as it depends on the TiO_2/g-CN ratios.[13] Future works will focus on the formation of TiN macro-/nanostructures without the residual carbon through further synthetic design.

ASSOCIATED CONTENT

Supporting Information. bmp-TiN/C synthesis methods, electrochemical analysis, discharge-charge curve, cyclability test, SEM/TEM images, XRD patterns, FT-IR and XPS spectra of bmp-TiN/C cathodes. This material is available free of charge via the Internet at http:// pubs.acs.org.

AUTHOR INFORMATION

E-mail: youngsi.jun@gmail.com (Y.-S. Jun); stucky@chem.ucsb.edu (G. D. Stucky).

ACKNOWLEDGMENT

This work is supported by the University of California Lab Fees Research Program and the MRSEC Program of the National Science Foundation (DMR 1121053). W.-r. L. is supported by a Fulbright Fellowship and the National Science Foundation (DMR08-05148).

REFERENCES

(1) Bruce, P. G.; Freunberger, S. A.; Hardwick, L. J.; Tarascon, J.-M. Nat. Mater. 2012, 11, 19.

(2) Jung, H.-G.; Hassoun, J.; Park, J.-B.; Sun, Y.-K.; Scrosati, B. Nat. Chem. 2012, 4, 579.

(3) Ottakam Thotiyl, M. M.; Freunberger, S. A.; Peng, Z.; Bruce, P. G. J. Am. Chem. Soc. 2012, 135, 494.

(4) Black, R.; Lee, J.-H.; Adams, B.; Mims, C. A.; Nazar, L. F. Angew. Chem. 2013, 125, 410.

(5) Qi, H.; Roy, X.; Shopsowitz, K. E.; Hui, J. K. H.; MacLachlan, M. J. Angew. Chem. Int. Ed. 2010, 49, 9740.

(6) Chen, H.; Nambu, A.; Wen; Graciani, J.; Zhong; Hanson, J. C.; Fujita, E.; Rodriguez, J. A. J. Phys. Chem. C 2006, 111, 1366.

(7) Fischer, A.; Antonietti, M.; Thomas, A. Adv. Mater. 2007, 19, 264.

(8) Isogai, S.; Ohnishi, R.; Katayama, M.; Kubota, J.; Kim, D. Y.; Noda, S.; Cha, D.; Takanabe, K.; Domen, K. Chem. Asian J. 2012, 7, 286.

(9) Li, F.; Ohnishi, R.; Yamada, Y.; Kubota, J.; Domen, K.; Yamada, A.; Zhou, H. Chem. Commun. 2013, 49, 1175.

(10) Jun, Y. -S.; Hong, W. H.; Antonietti, M.; Thomas, A. Adv. Mater. 2009, 21, 4270.

(11) Jun, Y.-S.; Park, J.; Lee, S. U.; Thomas, A.; Hong, W. H.; Stucky, G. D. Angew. Chem. Int. Ed. http://dx.doi.org/10.1002/anie.201304034.

(12) McCloskey, B. D.; Scheffler, R.; Speidel, A.; Bethune, D. S.; Shelby, R. M.; Luntz, A. C. J. Am. Chem. Soc. 2011, 133, 18038.

(13) Fischer, A.; Jun, Y.-S.; Thomas, A.; Antonietti, M. Chem. Mater. 2008, 20, 7383.

Jihee Park, Young-Si Jun,* Woo-ram Lee, Jeffrey A. Gerbec, Kimberly A. See, and Galen D. Stucky*

Chem. Mater. **2013**,

Bimodal Mesoporous Titanium Nitride/Carbon Microfibers as Efficient and Stable Electrocatalysts for Li-O_2 Batteries